Journal of Applied Mechanics and Technical Physics, Vol. 44, No. 3, pp. 365–372, 2003

EFFECT OF BOUNDARY-LAYER THICKNESS ON THE STRUCTURE OF A NEAR-WALL FLOW WITH A TWO-DIMENSIONAL OBSTACLE

V. V. Larichkin[1] **and S. N. Yakovenko**[2]

UDC 532.526.4

Results of physical and numerical experiments on investigating the effect of the depth of immersion of a two-dimensional obstacle with a square cross section into a developed turbulent boundary layer on the length of the separated flow region are presented. The numerical simulation is based on solving averaged Navier–Stokes equations with the use of the k–ε model of turbulence. The near-wall flow is visualized in the experiments, and the fields of mean and fluctuating velocities are measured. Flow regions where the results of numerical simulation agree with experimental data are determined. It is shown that the length of the recirculation flow region in the near wake increases with decreasing depth of immersion of the two-dimensional obstacle into the turbulent boundary layer.

Key words: *turbulent boundary layer, two-dimensional obstacle, experiment, numerical simulation.*

Introduction. The study of flow separation from the body surface and the resultant separated flow is of significant theoretical and applied importance. Separated flows emerge in ducts of various engineering devices, in the wind flow around ground-based structures, and in motion of flying vehicles, cars, and trains.

Of special interest is the study of the flow around various steps and superstructures, which are structural elements or specially mounted devices, for instance, for the purpose of intensification of mixing and combustion. The complexity and variety of separated flows encountered in reality require a detailed study of their characteristic regions: separation, mixing, reattachment, reverse flow, boundary-layer recovery, etc. (Fig. 1).

There are many experimental works dealing with the separated flow around two- and three-dimensional obstacles on flat and curved surfaces. In some papers (see, e.g., [1]), the properties of low-amplitude perturbations developed in the vicinity of a two-dimensional obstacle located in the laminar boundary layer on a flat plate were considered. The object of investigation in other papers (see, e.g., [2]) was the action of a two-dimensional roughness element on the developed boundary layer. At the same time, the influence of the depth of immersion of the obstacle into the shear flow on the separation region was not considered.

It should be noted that the mathematical solution of the problem of description of turbulent separated flows near bluff bodies involves large difficulties. Three main directions of calculating separated flows have been currently formed: 1) approximate calculations with the use of integral and asymptotic methods [3, 4]; 2) the use of the unsteady vortex model of an inviscid liquid [5]; 3) numerical studies by solving the Navier–Stokes or Reynolds equations [6–10]. In solving some problems, for instance, those related to flow separation near steps, the method of coarse particles is used [11]. At the same time, many problems of the theory of separated flows remain unsolved. Two-dimensional [3, 7, 10] and three-dimensional [8, 9] turbulent flows near obstacles on a flat surface were calculated, but the results of these calculations do not agree with acceptable accuracy with the measurement data. This circumstance defined the objective of the present study and the complex approach to solving the problem: physical and numerical experiment.

[1]Novosibirsk State Technical University, Novosibirsk 630092. [2]Institute of Theoretical and Applied Mechanics, Siberian Division, Russian Academy of Sciences, Novosibirsk 630090. Translated from Prikladnaya Mekhanika i Tekhnicheskaya Fizika, Vol. 44, No. 3, pp. 76–84, May–June, 2003. Original article submitted October 2, 2002; revision submitted November 4, 2002.

0021-8944/03/4403-0365 $25.00

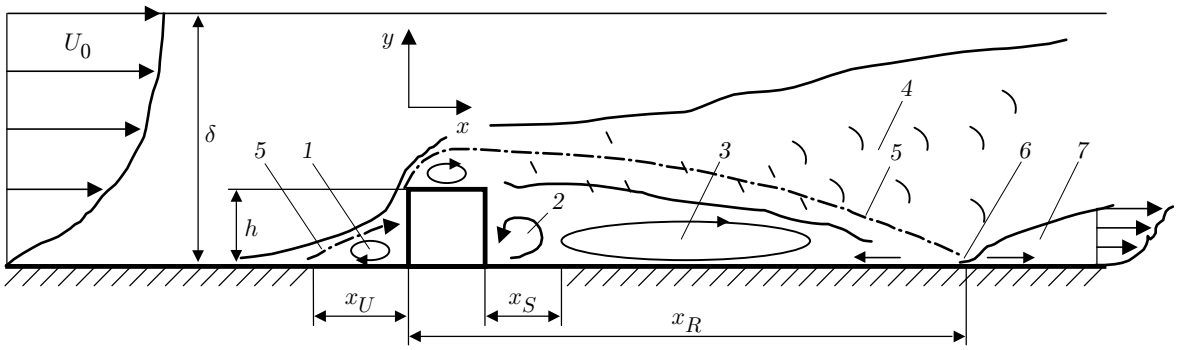

Fig. 1. Flow pattern around an obstacle on a flat surface: 1) recirculation region upstream of the obstacle; 2) region of the small vortex behind the obstacle; 3) large recirculation region behind the obstacle; 4) mixing layer; 5) streamline $\psi = 0$; 6) region of flow reattachment to the wall; 7) recovering boundary layer.

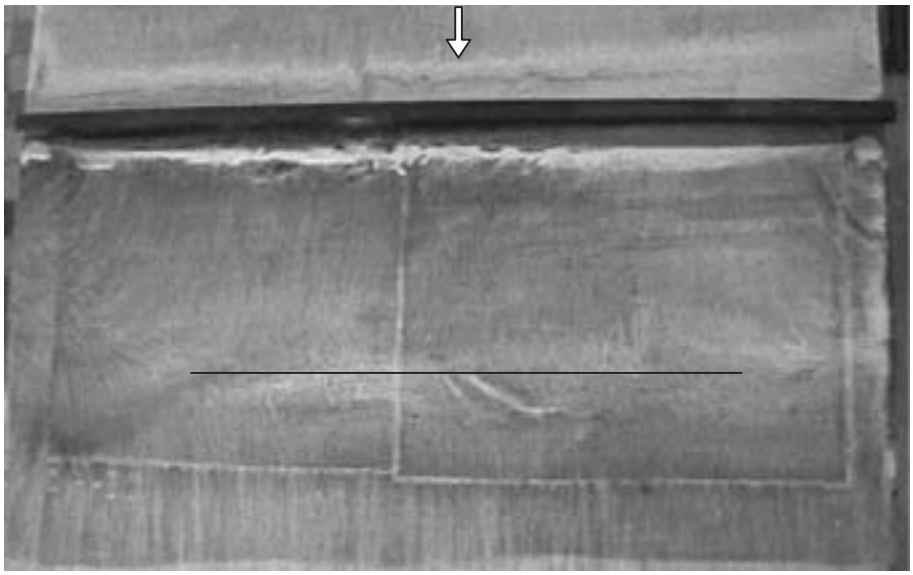

Fig. 2. Flow pattern in the vicinity of the two-dimensional obstacle of square cross section ($h = 20$ mm, $h/\delta = 1.44$, and $\mathrm{Re}_h \approx 17,000$).

The present paper deals with experimental and numerical investigations of a subsonic flow around two-dimensional obstacles of square cross section on a flat surface, which are partly or completely immersed into the developed turbulent boundary layer, in the absence of sideslip.

1. Experimental Technique. The experiments were performed in a T-324 low-turbulent subsonic wind tunnel of the Institute of Theoretical and Applied Mechanics of the Siberian Division of the Russian Academy of Sciences. This wind tunnel has a square test section 1×1 m and a length of 4 m. The obstacle models were wooden cylinders of square cross section (40×40, 20×20, and 10×10 mm) located on the test-section wall at a distance of 2.81 m from the nozzle exit or on a flat plate 1.5 m long at a distance of 0.6 or 0.9 m from the leading edge. A detailed description of test conditions and measurement technique can be found in [12]. A two-dimensional obstacle is understood as a model set against the side walls of the wind tunnel (the ratio of the test-section height H to the obstacle height h varied from 25 to 100, i.e., was rather large). The experiments were performed for free-stream velocities $U_0 = 25$ and 45 m/sec. The Reynolds numbers based on the obstacle height were within the range $\mathrm{Re}_h = 17,000$–$123,000$. In all cases, an equilibrium turbulent boundary layer with a power law of velocity distribution (with an exponent close to 1/7) was formed at the point where the obstacle was located. The degree of free-stream turbulence was $\varepsilon_u \leqslant 0.08\%$.

The flow was visualized by the oil-film technique, and the fields of mean and fluctuating velocities in the streamwise direction were measured by hot-wire anemometry by a miniature single-wire sensor with allowance for methodical recommendations of [13].

2. Flow Structure. Figure 2 shows an example of visualization of the flow around a two-dimensional obstacle of square cross section partly immersed into a turbulent boundary layer, at zero sideslip. It is seen that the flow is quasi-two-dimensional in the major part of the channel. An analysis of a large number of near-wall flow patterns shows that the greater the ratio H/h, i.e., aspect ratio, the greater the region of quasi-two-dimensionality. At the same time, the effect of the side walls of the wind tunnel, which is manifested in the presence of powerful vertical vortices at the ends, affects the length of the recirculation flow region.

Figures 3 and 4 show the profiles of mean velocities and intensity of root-mean-square fluctuations at different relative distances x/h upstream and downstream of the obstacle. A comparison of the distributions of mean velocities and their fluctuations in the presence and absence of the obstacle shows that the obstacle in the boundary layer significantly transforms the shape of the profiles. As the flow approaches the obstacle, because of the decelerating action of the latter, the mean velocity near the surface becomes significantly lower, an inflection appears on the profile, which indicates that the streamlines move away from the surface and a separated flow is formed, and velocity fluctuations increase. A wide separation region is formed behind the obstacle, the turbulent boundary layer being recovered behind this region. As a whole, this pattern is in agreement with that shown in Fig. 1.

An analysis of spectral patterns of perturbations in the wake behind the obstacle for different values of the x and y coordinates indicates the absence of coherent structures of the type of the Kármán vortex street, which agrees with the data of [13]. Apparently, this is associated with substantial stochastization of the flow because of the interaction of shear layers separated from the obstacle with the flat surface.

3. Numerical Simulation. To obtain a mathematical description of the structure of the turbulent flow around the two-dimensional obstacle, we used the continuity and Navier–Stokes equations averaged over an ensemble of instantiations, which allow calculation of the mean pressure and components of the mean velocity vector. The system of equations of turbulent transfer for a two-dimensional unsteady incompressible liquid flow has the form

$$\frac{\partial U}{\partial x}+\frac{\partial V}{\partial y}=0,$$

$$\frac{\partial U}{\partial t}+\frac{\partial U^2}{\partial x}+\frac{\partial (UV)}{\partial y}=\frac{\partial}{\partial x}\Big[2\nu_{\text{eff}}\,\frac{\partial U}{\partial x}\Big]+\frac{\partial}{\partial y}\Big[\nu_{\text{eff}}\Big(\frac{\partial U}{\partial y}+\frac{\partial V}{\partial x}\Big)\Big]-\frac{\partial}{\partial x}\Big(\frac{P}{\rho}+\frac{2}{3}\,k\Big),$$

$$\frac{\partial V}{\partial t}+\frac{\partial (UV)}{\partial x}+\frac{\partial V^2}{\partial y}=\frac{\partial}{\partial y}\Big[2\nu_{\text{eff}}\,\frac{\partial V}{\partial y}\Big]+\frac{\partial}{\partial x}\Big[\nu_{\text{eff}}\Big(\frac{\partial U}{\partial y}+\frac{\partial V}{\partial x}\Big)\Big]-\frac{\partial}{\partial y}\Big(\frac{P}{\rho}+\frac{2}{3}\,k\Big), \tag{1}$$

$$\frac{\partial k}{\partial t}+\frac{\partial (kU)}{\partial x}+\frac{\partial (kV)}{\partial y}=\frac{\partial}{\partial x}\Big[\nu_k\,\frac{\partial k}{\partial x}\Big]+\frac{\partial}{\partial y}\Big[\nu_k\,\frac{\partial k}{\partial y}\Big]+P_k-\varepsilon,$$

$$\frac{\partial \varepsilon}{\partial t}+\frac{\partial (\varepsilon U)}{\partial x}+\frac{\partial (\varepsilon V)}{\partial y}=\frac{\partial}{\partial x}\Big[\nu_\varepsilon\,\frac{\partial k}{\partial x}\Big]+\frac{\partial}{\partial y}\Big[\nu_\varepsilon\,\frac{\partial k}{\partial y}\Big]+(C_{\varepsilon 1}P_k-C_{\varepsilon 2}\varepsilon)\,\frac{\varepsilon}{k},$$

where U and V are the velocity-vector components in the x and y directions, respectively, $\nu_{\text{eff}}=\nu+\nu_{\text{t}}$, $\nu_k=\nu+\nu_{\text{t}}/\sigma_k$, and $\nu_\varepsilon=\nu+\nu_{\text{t}}/\sigma_\varepsilon$ are the effective diffusion coefficients ($\nu_t=C_\mu k^2/\varepsilon$ is the turbulent viscosity).

Generation of turbulent energy has the form

$$P_k=\nu_t\Big[2\Big\{\Big(\frac{\partial U}{\partial x}\Big)^2+\Big(\frac{\partial V}{\partial y}\Big)^2\Big\}+\Big(\frac{\partial U}{\partial y}+\frac{\partial V}{\partial x}\Big)^2\Big].$$

In system (1), ρ is the density, x and y are the horizontal and vertical coordinates, respectively, t is the time, and ν is the molecular viscosity.

The viscous sublayer was not resolved because of the high Reynolds numbers Re_h; therefore, the model has no corrections for the influence of the wall (low Reynolds numbers), and the boundary conditions near the solid surfaces are determined in the form of the power laws of the wall as

$$U_\tau(x_n)=\alpha x_n^{1/4},\quad U_n=0,\quad \frac{\partial k}{\partial x_n}=0,\quad \varepsilon(x_n)=\frac{2C_\mu^{3/4}(k(x_n))^{3/2}}{\gamma x_n},\quad \gamma=0.4,$$

where U_n and U_τ are the normal and tangential-to-wall components of the mean velocity vector; the coordinate axis x_n is directed normal to the wall ($x_n=x$, $U_n=U$, and $U_\tau=V$ on the vertical surfaces of the obstacle; $x_n=y$, $U_n=V$, and $U_\tau=U$ on the underlying horizontal surface and upper surface of the obstacle).

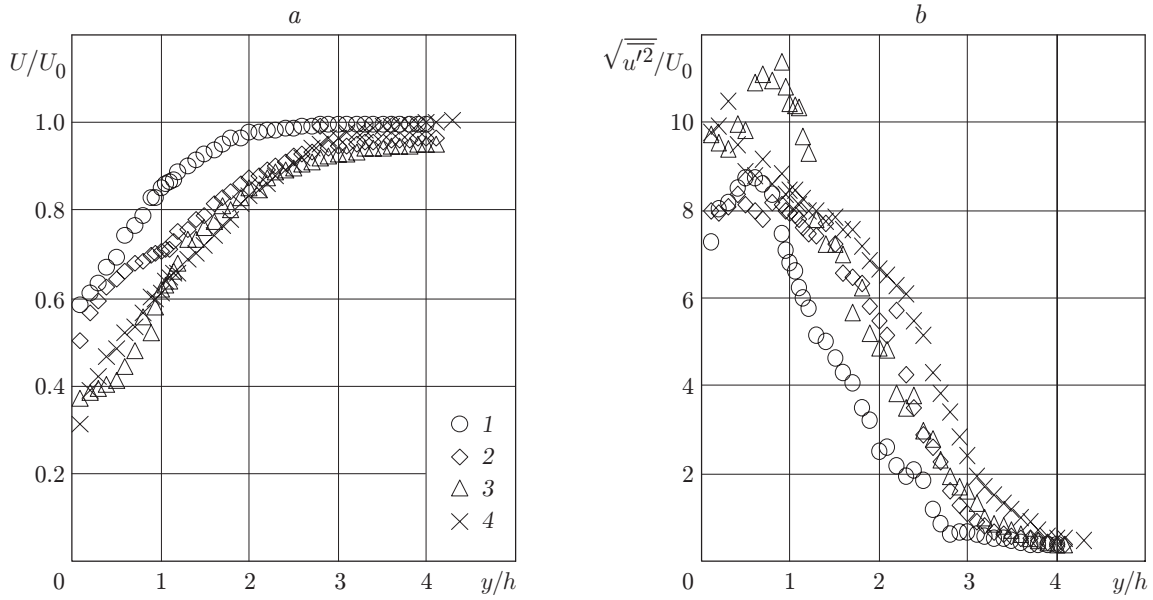

Fig. 3. Profiles of mean velocity (a) and fluctuations of the streamwise component of velocity (b) upstream of the two-dimensional obstacle ($h = 20$ mm, $z/L = 0.5$, and $L = 1$ m): $x/h = -15$ (1), -4.5 (2), -3 (3), and -1.5 (4).

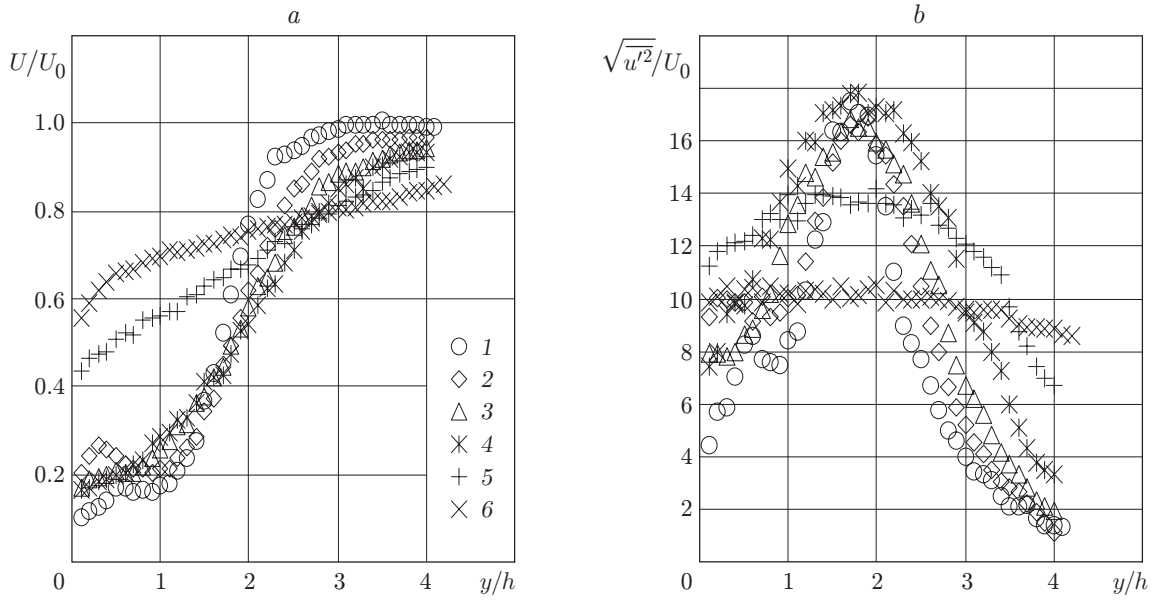

Fig. 4. Profiles of mean velocity (a) and fluctuations of the streamwise component of velocity (b) downstream of the two-dimensional obstacle ($h = 20$ mm, $z/L = 0.5$, and $L = 1$ m): $x/h = 2$ (1), 4 (2), 8 (3), 12 (4), 25 (5), and 50 (6).

The data at the input (upstream) boundary were specified on the basis of experimental results of the present work and [12], experiments of [13], and calculation of a developed turbulent boundary layer on a flat plate (without obstacles) of a given thickness (see, e.g., [14]). It should be noted that the experimental data of [12, 13] were obtained in the same T-324 wind tunnel under similar free-stream conditions. The experimental profiles of velocity and streamwise intensity of turbulence in the boundary layer on a flat plate [13] were approximated by the analytical functions

$$U(y) = U_0(y/\delta)^{1/5}, \quad y < \delta, \qquad U(y) = U_0, \quad y \geqslant \delta,$$
$$\sqrt{\langle u^2 \rangle}(y) = U_0\{0.0008 + 0.07(y/\delta)^{-1/9} \exp\left[-0.00081(y/\delta)^4\right]\}. \tag{2}$$

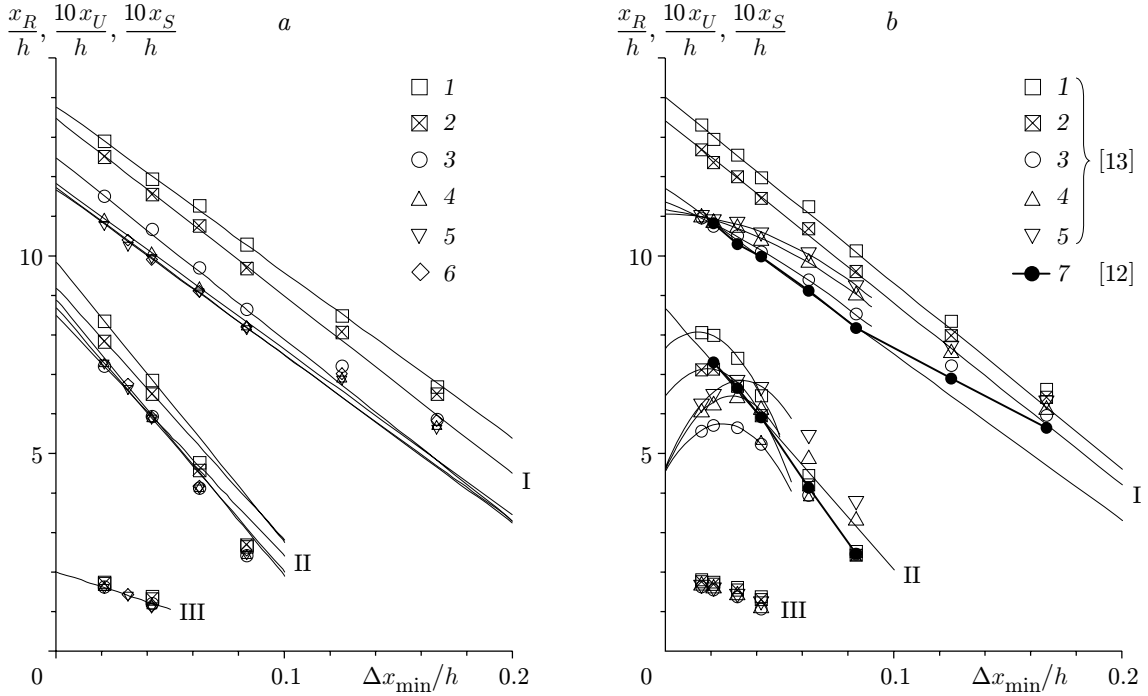

Fig. 5. Extrapolation of the recirculation-region length with grid refinement: the input profiles were obtained in computations without the obstacle (a) and based on the data of [12, 13] (b) for x_R/h (I), $10x_U/h$ (II), and $10x_S/h$ (III): $\delta/h = 0.35$ (1), 0.55 (2), 2.25 (3), 7.0 (4), 10.0 (5), 14.0 (6), and 2.25 (7).

The turbulent kinetic energy was found from the isotropic relation $k(y) = 1.5\langle u^2\rangle(y)$, and viscous dissipation

$$\varepsilon(y) = C_\mu^{1/2} k(y) \frac{\partial U}{\partial y} = \frac{1}{5} C_\mu^{1/2} k(y) \frac{U(y)}{y/\delta}, \quad y < \delta, \qquad \varepsilon(y) = \frac{1}{5} C_\mu^{1/2} k(y), \quad y \geqslant \delta$$

was obtained from the condition of local equilibrium $P_k(y) = \varepsilon(y)$ outside the viscous sublayer.

At the output (downstream) boundary, zero derivatives along the normal to the boundary were set for all the sought quantities, which corresponds to the flow region where the influence of the obstacle either is not manifested at all or is weak. At the upper boundary of the flow, zero gradients normal to the boundary and zero vertical velocity were prescribed. This statement of the problem corresponds to a negligibly small effect of the obstacle at the upper boundary located in the undisturbed free stream far from the wind-tunnel walls.

The numerical algorithm of implementation of the reduced k–ε model of turbulence, which employs time relaxation for the steady problem considered, is described in detail in [10]. The governing system (1) with the boundary conditions formulated above was solved under the test conditions described and those of [12] with different ratios of the obstacle height to the boundary-layer thickness upstream of the obstacle h/δ.

For each value of h/δ, a series of computations was performed on nonuniform grids condensing toward the obstacle and differing from each other by the minimum interval $\Delta x_{\min} = \min(x_{i+1} - x_i; y_{j+1} - y_j)$, namely, $h/\Delta x_{\min} = 6$, 8, 12, 16, 24, 32, 48, and 64. The computations show (see also [8, 10]) that the computational error decreases with increasing number of nodes of the difference grid and become localized at the upper face of the obstacle. The results of these computations can be used to determine the length of recirculation regions x_R, x_S, and x_U more exactly (see Fig. 1). Having a sufficient number of points, we can extrapolate the dependence shown in Fig. 5 to the case of an infinitely fine grid (inaccessible for computer resources) as $(\Delta x_{\min}/h) \to 0$.

Figure 5 shows the extrapolation of the recirculation-region length for two variants of the input boundary conditions. The curvature of extrapolation curves for input profiles interpolating the data of [13] for the boundary layer on a flat plate is caused by the absence of measurements near the underlying surface. In addition, it is known that the distribution of the mean and fluctuating characteristics of the velocity field in the viscous sublayer and buffer zone differ from the distributions in the logarithmic layer and wake region. Therefore, the uncertainty in measurement data near the wall can be the reason for inaccuracy of relations (2).

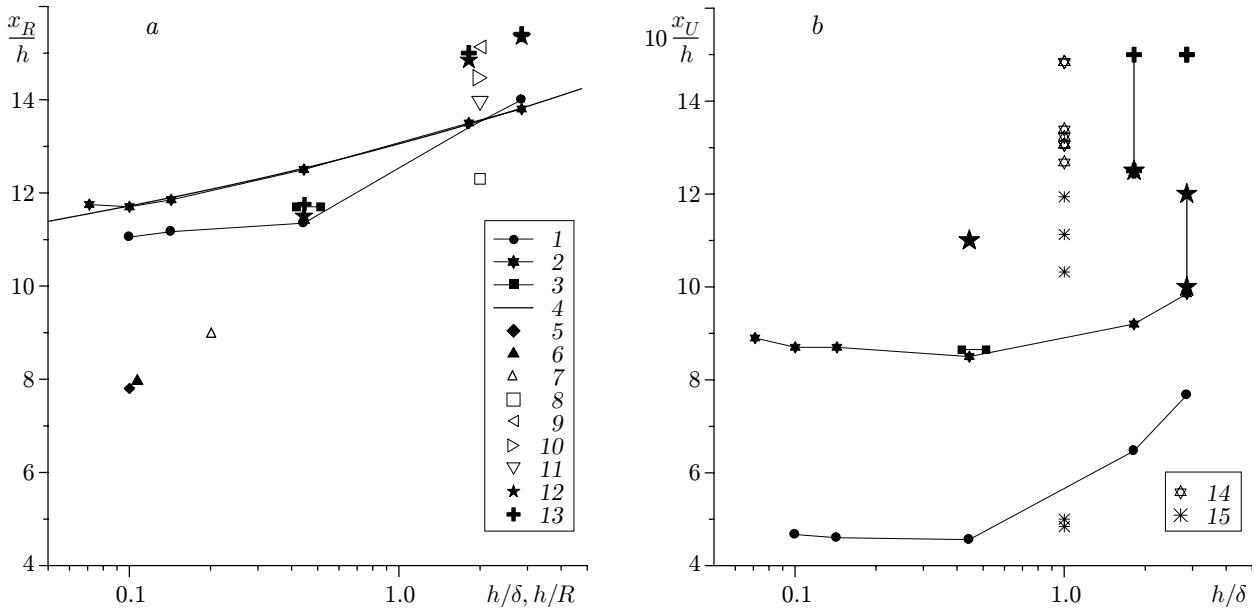

Fig. 6. Recirculation-region length downstream (a) and upstream (b) of the obstacle as a function of the relative thickness of the turbulent boundary layer: curves 1–4 refer to computations of the present work for $h/H = h/W = 0$ [input profiles obtained in computations without the obstacle (1), input profiles obtained by the data of [13, 12] (2 and 3), and interpolation curve (4)]; points 5–15 are the experimental data for $h/R = 0.100$ and $h/W \approx h/(2\pi R) = 0.016$ [15] (5), $h/R = 0.107$ and $h/W \approx 0.017$ [2] (6), $h/R = 0.201$ and $h/W \approx 0.032$ [2] (7), $h/H = 0.078$ [7] (8), $h/W = 0.025$ [16] (9–11) [$h/H = 0.067$ (9), $h/H = 0.051$ (10), and $h/H < 0.028$ (11)], $h/W = 0.02$ [12] (12, 13) [$h/H = 0.04$, $h/\delta < 2.25$, and $U_0 = 45$ m/sec (12) and $h/H = 0.02$, $h/\delta = 2.25$, and $U_0 = 25$ m/sec (13)], $h/H = 0.5$ and $h/W = 0.042$–0.500 [17] (14, 15) [oil-film visualization in an air flow (14) and visualization by crystals in a water flow (15)].

4. Results. Figure 6 shows the recirculation-region lengths x_R and x_U as functions of the relative boundary-layer thickness. The values of x_R and x_U are obtained by means of the extrapolation described above (see Fig. 5). The results of computations and various experiments described in [2, 12, 13, 15–17] for the boundary layer with an obstacle and the turbulent flow in a tube with a circular step of square cross section are plotted as functions of the ratio of the obstacle height h to the boundary-layer thickness δ (or to the tube radius R).

In addition to h/δ, the recirculation-region size can be significantly affected by other parameters, for instance, the blockage coefficient, which is the ratio of the obstacle height to the channel height h/H (or to the tube radius h/R). It was found [16] that the quantity x_R is a decreasing function of h/H [in Fig. 6a, points 9, 10, and 11 obtained in these experiments correspond to $h/H = 0.067$, 0.051, and <0.028 ($h/\delta = 0.5$)]. The influence of the parameter h/H on x_R starts to manifest for $h/H > 0.04$; for $h/H \approx 0.5$, the value of x_R decreases almost twofold as compared to the case $h/H \approx 0$ [16].

Thus, lower values of x_R for the flow in a plane channel for $h/H = 0.078$ [7] and the flow in a cylindrical tube for $h/R = 0.1$ [15], 0.107, and 0.201 [2], as compared to the case $h/H \to 0$, are caused by the damping effect of the opposite walls. It should be noted that the results of the present measurements and the data given in [12] were obtained for $h/H = 0.04$ (for $h/\delta = 0.35$ and 0.55) and 0.02 (for $h/\delta = 2.25$), i.e., the influence of the blockage coefficient on these data can be considered as insignificant.

An analysis of the dependence of x_R/h on h/δ with allowance for the blockage coefficient shows that the length of the recirculation region behind the obstacle increases with decreasing relative thickness of the boundary layer. A similar effect was also registered in [2, 12, 18]. We can assume that this effect is associated with more intense turbulent mixing in the case of a thicker shear layer (incoming onto the obstacle), which has larger energy-containing turbulent vortices with diameters of the order of the boundary-layer thickness. As a result, more intense mixing affecting the recirculation region through the turbulent mixing layer formed above this region provides more intense destruction of the recirculation reverse flow caused by a significant difference in pressure on the obstacle. A similar behavior is observed in varying the turbulence intensity at the input (see, e.g., [9]): the recirculation-region length decreases with increasing turbulence intensity.

Regardless of the shape of the input profiles and as a confirmation of experimental results, the present computations give a good description of the dependence of x_R/h on h/δ. The constancy (see Fig. 6) of the calculated values of x_R/h for small h/δ, which was also obtained in [18] for a two-dimensional obstacle of square cross section in the boundary layer with a positive pressure gradient (for $h/\delta < 0.15$), can be explained by the following assumption. When the characteristic size of large-scale turbulent vortices becomes significantly greater than the recirculation-region height, the latter ceases to change with further enlargement of these vortices.

The change in the calculated length of the recirculation region upstream of the obstacle with variation of the characteristic size of the energy-containing turbulent vortices seems to be observed only for $h/\delta > 1$, whereas the values of x_U/h calculated for $h/\delta < 1$ are almost constant (see Fig. 6). In addition, for the region upstream of the obstacle, the blockage coefficient and the ratio h/W (quantity inverse to the aspect ratio) should be much higher ($h/W > 0.5$) than those for the region downstream of the obstacle ($h/W > 0.1$) [17]; then, these parameters exert a significant effect on the value of x_U.

The data in Fig. 6 were obtained for different input profiles for the sought functions (horizontal mean velocity, turbulent kinetic energy, and its viscous dissipation rate) used in computations. Generation of these profiles from the numerical solution of the problem for a turbulent boundary layer on a flat plate without an obstacle yields a greater size of the recirculation region than in the case of specifying the experimental input profiles for U and $k = 1.5\langle u^2 \rangle$ (and also for dissipation ε determined by the locally equilibrium approximation $P = \varepsilon$). This difference is partly related to the lower intensity of turbulence in the case of the calculated input profiles. In addition, in the latter case, it is possible to obtain a more smooth dependence of x_R/h on h/δ. In particular, the function $x_R/h = 8.3 + 4.75(h/\delta)^{1/7}$ (curve 4 in Fig. 6a) offers a good description of the calculated dependence $x_R(\delta)$ outside the region of "saturation" of the function considered.

Conclusions. The results of the present investigations show that the flow around a two-dimensional obstacle partly or completely immersed into a turbulent boundary layer contains regions of quasi-two-dimensional flow; the size of these regions can be determined by using two-dimensional mathematical models. The reattachment region of the separated flow depends on the depth of immersion of the obstacle into the boundary layer. The distance is $x_R/h = 11$–12 for $h/\delta \leqslant 0.5$ and $x_R/h = 13$–15 for $h/\delta > 0.5$.

This work was supported by the Russian Foundation for Fundamental Research (Grant Nos. 99-05-64143 and 00-15-96164) within the framework of the Integration Project No. 1 (2000) of the Siberian Division of the Russian Academy of Sciences.

REFERENCES

1. P. S. Klebanoff and K. D. Tidstrom, "Mechanism by which a two-dimensional roughness element induces boundary-layer transition," *Phys. Fluids*, **15**, No. 7, 1173–1188 (1972).
2. W. H. Schofield and E. Logan, "Turbulent shear flow over surface mounted obstacles," *Trans. ASME, J. Fluids Eng.*, **112**, 376–385 (1990).
3. L. J. S. Bradbury, F. Durst, B. E. Launder, F. W. Schmidt, and J. H. Whitelaw (eds.), *Turbulent Shear Flows Springer-Verlag*, Berlin, Heidelberg, Vol. 1 (1979); Vol. 2 (1980).
4. V. V. Sychev, A. I. Ruban, V. V. Sychev, and G. L. Korolev, *Asymptotic Theory of Separated Flows* [in Russian], Nauka, Moscow (1987).
5. L. V. Gogish and G. Yu. Stepanov, *Separated and Cavitation Flows: Basic Properties and Numerical Models* [in Russian], Nauka, Moscow (1990).
6. O. M. Belotserkovskii, "Numerical experiment. Direct numerical simulation of complicated flows of gas dynamics on the basis of the Euler, Navier–Stokes, and Boltzmann equations," in: *Direct Numerical Simulation of Gas Flows. Numerical Experiment in Gas Dynamics* [in Russian], Nauka, Moscow (1978), pp. 6–64.
7. R. W. Benodekar, A. J. H. Goddard, A. D. Gosman, and R. I. Issa, "Numerical prediction of turbulent flow over surface-mounted ribs," *AIAA J.*, **23**, 359–366 (1985).
8. S. Murakami and A. Mochida, "3-D numerical simulation of airflow around a cubic model by means of k–ε model," *J. Wind Eng. Ind. Aerodyn.*, **31**, 283–303 (1988).
9. D. A. Paterson and C. J. Apelt, "Simulation of flow past a cube in a turbulent boundary layer," *J. Wind Eng. Indust. Aerodyn.*, **35**, 149–176 (1989).
10. A. F. Kurbatskii and S. N. Yakovenko, "Numerical investigation of the turbulent flow around a two-dimensional obstacle in the boundary layer," *Teplofiz. Aéromekh.*, **3**, No. 2, 145–163 (1996).

11. O. M. Belotserkovskii and Yu. M. Davydov, *Method of Coarse Particles in Gas Dynamics* [in Russian], Nauka, Moscow (1982).
12. V. V. Larichkin, M. V. Litvinenko, and V. A. Shcherbakov, "Experimental study of the turbulent flow in the vicinity of a two-dimensional obstacle in the boundary layer," *Teplofiz. Aéromekh.*, **9**, No. 1, 73–85 (2002).
13. V. I. Kornilov and D. K. Mekler, "Investigation of the memory of the turbulent boundary layer to two-dimensional perturbations," Preprint No. 32-87, Inst. Theor. Appl. Mech., Sib. Div., USSR Acad. of Sci., Novosibirsk (1987).
14. A. F. Kurbatskii and S. N. Yakovenko, "Diffusion of the passive admixture from a line source in the neutral atmospheric near-Earth layer," *Izv. Ross. Akad. Nauk, Fiz. Atmosf. Okeana*, **35**, No. 4, 506–515 (1999).
15. E. Logan and P. Phataraphruk, "Mean flow downstream of two-dimensional roughness elements," *Trans. ASME, J. Fluids Eng.*, **2**, 149–153 (1989).
16. F. Durst and A. K. Rastogi, "Turbulent flow over two-dimensional fences," in: *Turbulent Shear Flows-2*, Springer-Verlag, Berlin (1980), pp. 218–232.
17. A. Larousse, R. Martinuzzi, and C. Tropea, "Flow around surface-mounted, three-dimensional obstacles," in: *Turbulent Shear Flows-8*, Springer-Verlag, Berlin (1993), pp. 127–139.
18. H. H. Nigim and D. J. Cockrell, "Effects caused by small discrete two-dimensional roughness elements immersed in turbulent boundary layers," *J. Fluid Mech.*, **153**, 17–30 (1985).